ACS Photonics

Letter

Cite This: ACS Photonics 2018, 5, 3970−3976

pubs.acs.org/journal/apchd5

Rabi Splitting in a Plasmonic Nanocavity Coupled to a WS_2 Monolayer at Room Temperature

Xiaobo Han,[†] Kai Wang,*[,‡] Xiangyuan Xing,[‡] Mengya Wang,[‡] and Peixiang Lu*[,†,‡]

[†]Laboratory of Optical Information Technology, Wuhan Institute of Technology, Wuhan 430205, China

[‡]Wuhan National Laboratory for Optoelectronics and School of Physics, Huazhong University of Science and Technology, Wuhan 430074, China

Supporting Information

ABSTRACT: A large Rabi splitting (~145 meV) is demonstrated in a plasmonic nanocavity coupled to a WS_2 monolayer at room temperature. The nanocavity is composed of a silver nanocube and a silver film with an Al_2O_3 spacer of a few nanometers, which belongs to a nanoparticle on mirror (NPoM) type. The surface plasmon resonance (SPR) of the nanocavity can be tuned by controlling the thickness of nanogap and the size of silver nanocubes, which allows to successively adjust the SPR to accurately match the exciton energy of WS_2 monolayers (2.02 eV). A mode splitting can be clearly observed from the dark-field scattering spectrum of the single hybrid nanocavity, which is ascribed to a strong coupling between the nanocavity mode and the excitonic mode. Furthermore, the anticrossing curves of the hybrid system are obtained by recording the scattering spectra with varied sizes of silver nanocubes, which further validate the interaction regime. It presents a strong coupling platform for two-dimensional monolayers, which is of potential applications of the development of hybrid nanostructure devices.

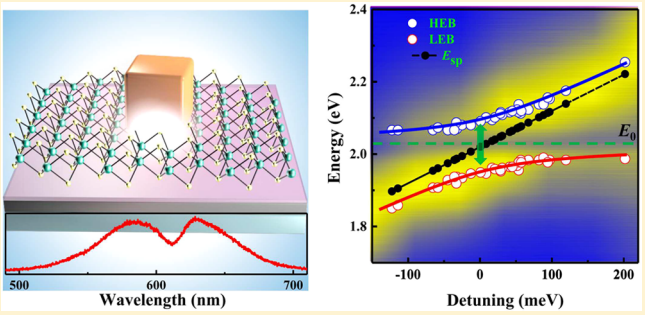

KEYWORDS: *strong coupling, Rabi splitting, plasmonic nanocavity, WS_2 monolayer, nanocube*

In recent years, strong light−matter interaction[1−3] has drawn much attention, which has potential applications in a low-threshold lasing and phase transition modification. Under this coupling, a new hybridization state is produced, where the wave functions of the initial emitter and the electromagnetic mode in a cavity are coherent superpositions.[3−5] Whereas most of hybrid nanostructures are working in a week coupling regime and only modify the exciton radiation efficiency to enhance photoluminescence (PL).[6−8] In order to achieve strong coupling, it is essential to have an emitter with a high oscillator strength and a high exciton binding energy (EBN). In particular, in order to obtain stable excitons at room temperature, it is not possible for strong coupling unless the EBN is larger than thermal loss rate (K_BT = 26 meV).[9] As it recently reported, quantum dots (QDs) and *J*-aggregates coupled to plasmon resonators have been observed strong coupling and Rabi splitting.[10−16] However, organic molecules tend to be photobleached and damaged, which is a key issue needed to be solved, while QDs are easily oxidized and agglomerated, which shows limitations for further applications.

Two-dimensional transition metal dichalcogenides (TMDs) open up a new research challenge on strong coupling. When the layer number of TMDs reduces to monolayer, band gap of TMDs transfers to the direct one.[17] Thus, it can enhance the interactions of dipole transitions with light, resulting in a high oscillator strength.[18] Importantly, the EBN in TMDs (e.g., WS_2 with 700 meV[19,20] at room temperature) is remarkably larger than the traditional semiconductors (e.g., ZnS with 40 meV, ZnO with 60 meV, GaN with 26 meV),[21,22] which makes the excitons more stable at room temperature. Moreover, TMDs provide homogeneous spatial distribution and well-defined in-plane orientated dipoles, which are essential for quantitative analysis. Therefore, TMDs monolayers have the potential for studying strong coupling with larger Rabi splitting at higher temperatures.

On the other hand, to reach the strong coupling regime, the coupling strength, g, should exceed both the cavity loss rate, κ, and the emitter scattering rate, γ, in order for energy to cycle back and forth between light and matter components, that is, $2g > \kappa,\gamma$.[2,9] Thus, specific resonators with high-Q ($Q \propto 1/\kappa$) for strong coupling is necessary. Moreover, since the coupling strength and mode volume are inverse-square ratios ($g \propto 1/\sqrt{V}$), a small cavity volume is also highly required to confine the excitons. Additionally, at room temperature, the splitting energy larger than the plasmon damping energy (~90 meV) is demanded.[23] Therefore, a high-Q−low-V cavity is required for realizing strong coupling. A possible solution to these challenges is that a plasmonic cavity could be used to

Received: July 10, 2018
Published: September 14, 2018

DOI: 10.1021/acsphotonics.8b00931
ACS Photonics 2018, 5, 3970−3976

instead the traditional ones, such as photonic crystal and microring resonator cavity, because metallic nanostructure has a unique ability to concentrate electromagnetic field within deep subwavelength scales.[24,25]

Recently, there is an increasing interest in the strong coupling between TMDs monolayers and plasmonic nanostructures.[20,23,26−30] Many works are primarily based on metal arrays for a convenient measurement,[20,30] which is an averaged effect ignoring individual characteristics. Also, it is a challenge to tune surface plasmon resonance (SPR) with a fixed particle arrays. Several groups have moved to a much smaller scale, investigating strong coupling between TMDs monolayers and individual metal nanoparticles (NPs).[26−29] It is quite convenient to tune the SPR by adjusting the NPs size and the refractive index of surrounding dielectric, providing an enlarged freedom to observe and control strong coupling, especially for TMDs. However, the nanocavity formed by individual NPs shows a limited ability of electric-field confinement and a relatively large cavity volume. It can be remarkably improved using an additional metal film with a nanospacer, known as the NPs on mirror (NPoM). It is equivalent to gap-mode patch antennas; thus, optical volume is allowed below 50 nm^3, even up to 1 nm^3.[9] In 2017, Jeremy groups reported a prospective study on strong coupling in NPoM coupled to TMDs with a gold nanosphere.[23] The strong local-field in NPoM is dominantly out-of-plane, and then the plasmons cannot couple well with the in-plane excitons of TMDs, therefore it can only be realized in TMDs with several layers (7 layer at least). To the best of our knowledge, the strong coupling from NPoM coupled to a TMDs monolayer is still unaddressed.

Here, we demonstrate a large Rabi splitting (~145 meV) in an NPoM plasmonic nanocavity coupled to a WS_2 monolayer at room temperature. The nanocavity is composed of a silver film and individual silver nanocubes with an Al_2O_3 spacer, which confines the electromagnetic field in a small volume. By controlling the thickness of the nanogap and the size of silver nanocubes, the SPR wavelength of the nanocavity can be easily tuned, which allows to successively adjust the SPR to accurately match the exciton energy of WS_2 monolayers. An obvious mode splitting is observed from the dark-field scattering spectrum at the single-particle level, which indicates the coherent interaction between the in-plane excitons and plasmons. Anticrossing behavior is also presented by changing the size of silver nanocubes, which further confirms the strong coupling mechanism. In addition, both scattering and absorption spectra numerical simulations are performed, and the results further validate the coupling regime in the hybrid system. It presents a new platform to realize strong coupling for two-dimensional materials, which has potential applications in manipulating the excitons in 2D monolayers at room temperature.

The cross-section diagram of the hybrid nanostructure is shown in Figure 1a. The plasmonic nanocavity consists of a single silver nanocube and a silver film. A thin spacer film (Al_2O_3) and WS_2 monolayers are embedded in the gap. The cavity resonance can be adjusted by controlling the spacer thickness and varying the nanocube size. Figure 1b shows the distribution of simulated electric field in the *xy*-plane at resonance in the plasmonic cavity, which is a dipole similar oscillation along the nanocube edge (for more details, see Figure S1).[31] The sub-10 nm vertical dimension of the cavity results in a large electric-field enhancement. WS_2 monolayers are grown on sapphire substrates by chemical vapor deposition (CVD).[32] The shapes of single crystalline WS_2 flakes are triangular, as shown in

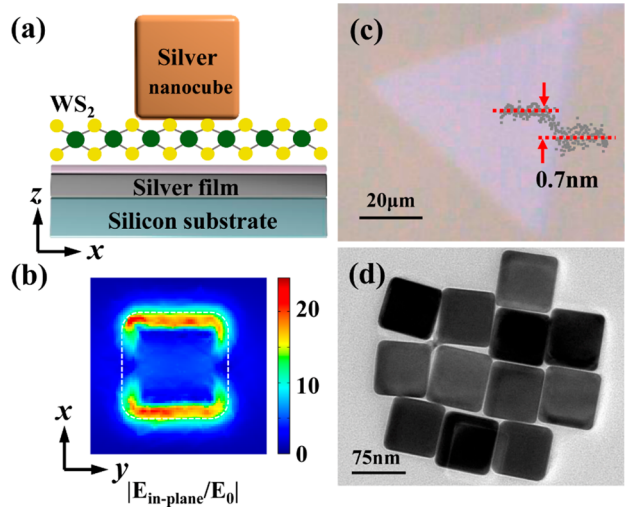

Figure 1. (a) Cross-section diagram of the hybrid nanostructures fabricated on a silicon substrate. Plasmonic nanocavity is composed of individual silver nanocubes and a silver film. WS_2 monolayers and a spacer film (Al_2O_3) embedded in the gap. (b) Calculated electric-field distribution in *xy*-plane in the plasmonic nanocavity. The incident light is polarized along the *x*-axis. White dashed lines indicate the outline of the silver nanocube. (c) Optical image of WS_2 monolayers on a sapphire substrate, showing a triangular shape with a side length of ~100 μm. The height profile of WS_2 flakes is characterized by AFM, which shows a ~0.7 nm thickness. (d) TEM image of silver nanocubes, indicating a cube shape with an edge length of ~75 nm.

Figure 1c. The monolayer characteristic is confirmed by atomic force microscopy (AFM), which demonstrates that the thickness of WS_2 flakes is ~0.7 nm.[33] Figure 1d shows transmission electron microscopy (TEM) image of the silver nanocubes, which represents the square shape and the edge length (~75 nm).

To characterize strong coupling for individual nanostructures, previous works show that single-particle dark-field scattering measurement is convenient.[11,13] Figure 2a illustrates the dark-field scattering experimental setup for individual silver nanocubes, where a dark-field objective is used to illuminate samples by an oblique white light and then collect the vertical scattering signals. Figure 2b shows a typical optical image of hybrid nanostructures, in which yellow section presents the WS_2 monolayer flakes and the small dots present individual nanocubes. The corresponding dark-field scattering image of the same sample is shown in Figure 2c. The boundary of the WS_2 monolayer appears a blue outline. Small bright spots indicate monodispersed silver nanocubes, which is one-to-one correspondence between Figure 2b,c. Thus, it indicates that a clear sample without dirt is prepared, which is an important guarantee for the scattering measurement. Details of the scattering experiment measurement are presented in the Methods section. Figure 2d shows the photoluminescence (PL) spectrum of a WS_2 monolayer excited by a He−Cd laser, which shows an exciton emission centering at 615 nm.[33] For matching the exciton energy of WS_2 monolayers, we tune the spacer thickness to adjust SPR wavelength of the plasmonic nanocavity. As shown in Figure 2e, with increasing the Al_2O_3 thickness from 6 to 10 nm, SPR peaks are tuned from 590 to 660 nm with a full width at half-maximum of ~50 nm. Note that more than 20 measurements of different silver nanocubes have been done for a thickness of Al_2O_3, and the related scattering spectrum shown in Figure 2e is the average value. When the Al_2O_3 thickness is ~7

DOI: 10.1021/acsphotonics.8b00931
ACS Photonics 2018, 5, 3970−3976

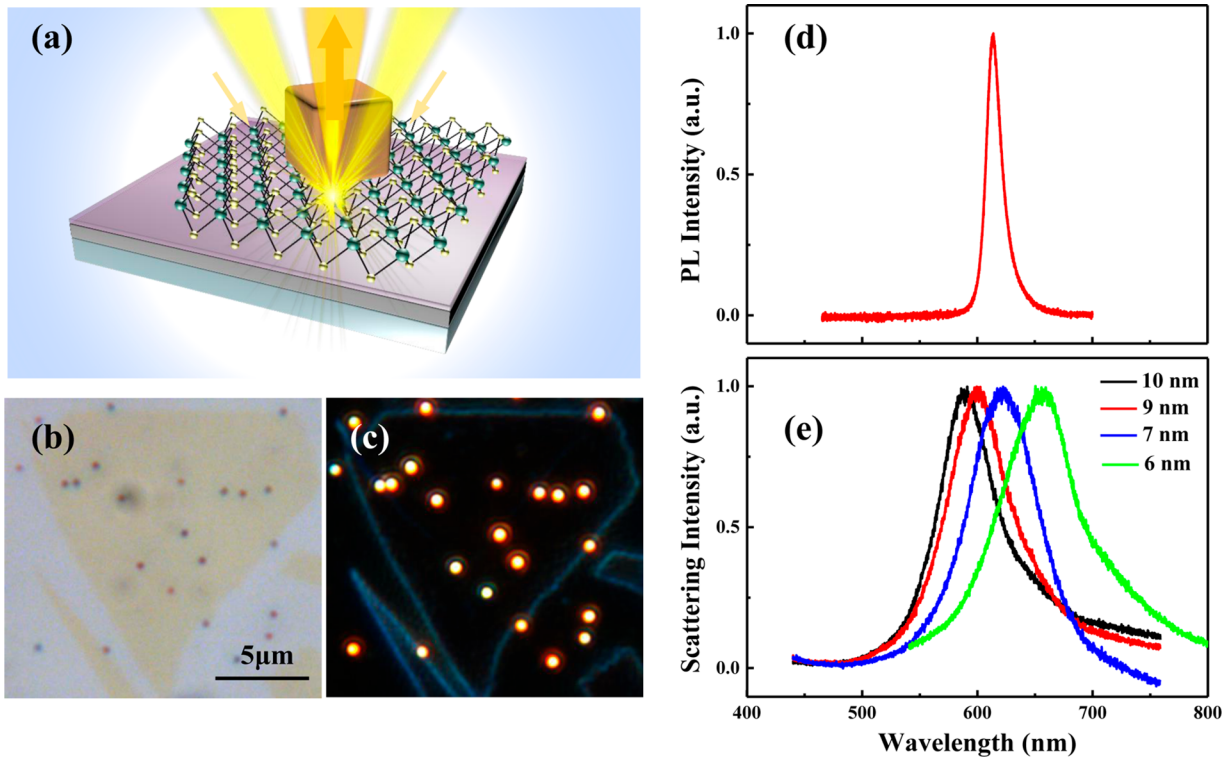

Figure 2. (a) Schematic experiment setup for measuring dark-field scattering signals of individual nanoparticles. Oblique incident white light illuminated the samples and vertical scattering signals are collected. (b) Bright-field optical image of the hybrid nanostructure, the yellow flakes represent the monolayer WS_2, and small dark dots represent individual silver nanocubes. (c) Dark-field microscope image corresponding to the same section of (b). Edges of WS_2 monolayers appears a blue outline, while bright spots indicate individual silver nanocubes. (d) PL spectrum of WS_2 monolayers excited with a He−Cd laser at room temperature. (e) Scattering spectra of the plasmonic nanocavities with various thickness of spacer Al_2O_3. When the Al_2O_3 thickness is adjusted to 7 nm, SPR is overlapped well with exciton energy in (d).

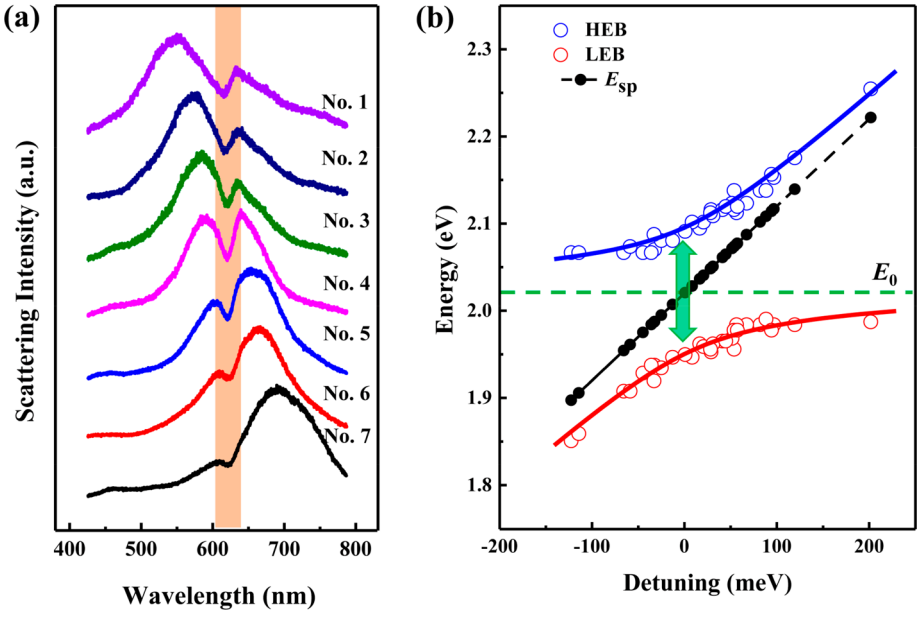

Figure 3. (a) Scattering spectra of the hybrid nanostructures with different size of silver nanocubes (sample numbers from 1 to 7). All spectra appear as two peaks and a dip at the exciton resonance of WS_2 monolayers. SPR wavelength of the plasmonic nanocavity is tailored across the exciton resonance of WS_2 monolayers. (b) Dispersion of plexciton with HEB and LEB varied as a function of detuning. Blue and red dots indicate experimental data extracted from scattering spectra. The solid lines are fits of the couple harmonic oscillator model. Black dots present the plasmon energy of the pure plasmonic nanocavity, while green dash line indicate the exciton resonance of WS_2 monolayers. Green arrows marked the Rabi splitting energy of the hybrid nanostructures, giving a splitting of ~145 meV.

DOI: 10.1021/acsphotonics.8b00931
ACS Photonics 2018, 5, 3970−3976

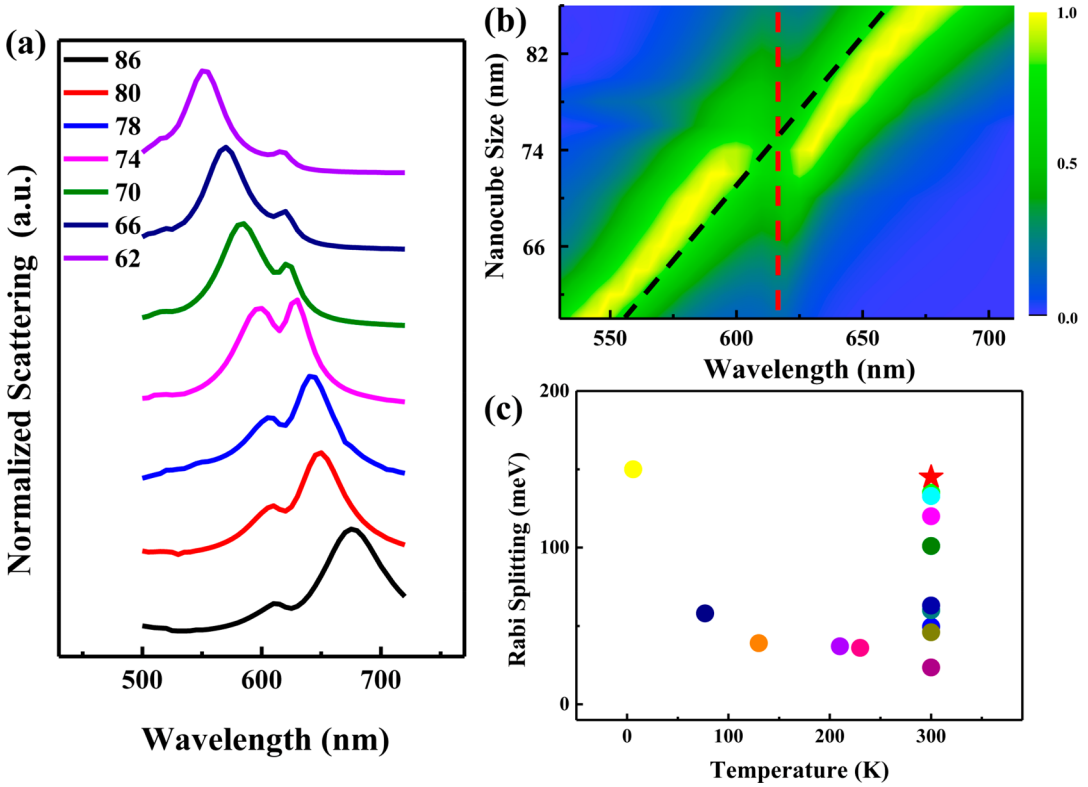

Figure 4. (a) Plot of the calculated scattering spectra of the hybrid nanostructures for different silver nanocube sizes (62−86 nm in cube length). Note that all the spectra have been normalized. (b) 2D contour plot of the calculated scattering spectra as a function of the size of silver nanocubes. Red and black lines indicate the position of uncoupled exciton and plasmon resonances, respectively. (c) Statistic of strong coupling based on TMDs as a function of temperature in recent experimental works.

nm, the wavelengths of SPR and PL are overlapped spectrally. Thus, the subsequent strong coupling is measured with the Al_2O_3 thickness of ∼7 nm.

After integrating the WS_2 monolayers under silver nanocubes, we measure the scattering spectra of hybrid nanostructures, as shown in Figure 3a. While keeping the thickness of spacer constant, scattering signals of silver nanocubes with varied size (65−95 nm) are measured. The scattering peaks progressively tuned across the PL peak. As a result of coupling, all normalized spectra show two peaks and a dip at the exciton resonance. In sample No. 4, spectra between SPR and PL are overlapped well, thus, the splitting appears a deeper dip and almost symmetric line shape. To map the dispersion curve, we extract the two peaks of multiple nanocubes scattering spectra, as marked in Figure 3b (blue and red dots). The traces of all peaks present an anticrossing curve across the zero detuning, containing high and low energy branches (HEB and LEB), respectively. The anticrossing behavior is a typical characteristic of the strong coupling between exciton and plasmon.[4,9,34] The coherent states can be described using a couple harmonic oscillator model as[26,27,35]

$$\begin{pmatrix} E_{SP} - i\gamma_{SP}/2 & g \\ g & E_0 - i\gamma_0/2 \end{pmatrix} \begin{pmatrix} \alpha \\ \beta \end{pmatrix} = E_{\pm} \begin{pmatrix} \alpha \\ \beta \end{pmatrix} \quad (1)$$

where E_{sp} and E_0 are the energies of the uncoupled plasmon and exciton energy, respectively; γ_{SP} and γ_0 are the dissipation rates of the uncoupled ones; g is coupling strength; and $E_{\pm}$ is the eigen energy of the hybrid nanostructure. Parameters α and β are the coefficients of the liner combination of the plasmon and exciton and satisfy $|\alpha|^2 + |\beta|^2 = 1$. By considering the detuning, the energy $E_{\pm}$ of the hybrid modes is obtained as

$$E_{\pm} = \frac{1}{2}\left[E_{SP} + E_0 \pm \sqrt{4g^2 + \left(\delta - \frac{i}{2}(\gamma_{SP} - \gamma_0)\right)^2}\right] \quad (2)$$

where $\delta = E_{SP} - E_0$ is the detuning energy between plasmon and exciton. The plasmon line width of the nanocavity γ_{SP} can be extracted to be ∼220 meV from Figure 2e. While for γ_0 of WS_2 monolayers, it is extracted to be ∼50 meV. Scattering peaks in Figure 3b can then be fitted by eq 2. The value E_0 is define as 2.02 eV, according to the PL data in Figure 2d. While for the value E_{SP} of each scattering spectra, it is calculated by $E_{SP} = E_+ + E_- - E_0$. Anticrossing fitting results are shown in Figure 3b (solid curves), which agrees well with the experimental data. Rabi splitting of hybrid nanostructure can be obtained as $\hbar\Omega = \sqrt{4g^2 - \frac{(\gamma_{SP} - \gamma_0)^2}{4}} = 145$ meV at $E_{SP} = E_0$. Thus, Rabi splitting energy fulfill the criterion where the strong coupling can occur $\hbar\Omega > \frac{\gamma_{SP} + \gamma_0}{2}$,[3,11,36] which indicates that the plasmon−exciton interactions satisfy the strong coupling regime.

The coupling strength as a function of exciton and cavity can be described as[9,11,28]

$$g = \mu_m \sqrt{\frac{4\pi\hbar Nc}{\lambda\varepsilon\varepsilon_0 V}} \quad (3)$$

where $\mu_m = 56D$ is the exciton transition dipole moment of WS_2 monolayers;[27] N, λ, ε, and V are the number and wavelength of exciton, dielectric function, and mode volume, respectively.

DOI: 10.1021/acsphotonics.8b00931
ACS Photonics 2018, 5, 3970−3976

Following previous study,[31] effective mode volume in the plasmonic nanocavity can be calculated as $V = 0.001(\lambda/n)^3$. Thus, the number of excitons contributing to the plexciton is only determined by the g value. Here, it is estimated about $N = 130$. If the nanocube size reduces, the exciton number could be further decreased and the hybrid nanostructure has the potential application on single or few excitons strong coupling mechanism.

To confidently identify the strong coupling regime, we calculate the scattering spectra in the plasmonic nanocavity with WS_2 monolayers by Comsol Multiphysics software under a linear plane wave with a normal incidence. The refractive indices of the WS_2 monolayers are measured by a ellipsometer (shown in Figure S2), which is agreed well with previous data.[20,33] The simulated results are shown in Figure 4a, which is recorded by adjusting the silver nanocube size. Figure 4a shows the normalized scattering spectra corresponding to the experimental data in Figure 3a. It indicates two peaks and one fixed dip at exciton resonance, which agrees well with the experimental data. For a clear anticrossing behavior, Figure 4b shows the 2D contour plot of simulated scattering spectra as a function of nanocube size. For some week couplings, such as enhanced absorption, exciton-induced transparency and Fano resonance,[37] they may also present mode splitting in scattering spectra. In order to further prove the strong coupling interaction, we complemented the scattering data with calculated absorption spectra (see Figure S3). The results also show large splitting and anticrossing behavior. For the case of a weak coupling system, the absorption spectra should show a single peak at the SPR or a weak dip around the exciton resonance.[38] Hence, these calculations provide additional evidence that the strong coupling scenario is indeed achieved.

Additionally, we list the experimental results in recent works on strong coupling of TMDs,[20,23,26−28,30,34,39−41] as shown in Figure 4b (detailed data listed in Table S1). With each Rabi splitting energy recorded by a dot as a function of temperature, its energy varied from several meV to ∼150 meV. Our result is marked by a red star. To the best of our knowledge, our result shows the largest Rabi splitting energy compared with the works on strong coupling of TMDs at room temperature, and it is even comparable to the result at 6 K.[28] In comparison to previous nanostructures (e.g., metal arrays and single NPs), the ultracompact plasmonic nanocavity (NPoM) provides a small volume and high-Q quality ($9 = E_0/\gamma_{SP}$). The coupling strength is determined by the cavity ability, which can be characterized by the ratio between Q and V. Lower cavity loss rate results in stronger coherent coupling between plasmon and exciton. In previous reports,[23] it presents strong coupling from NPoM with a gold nanosphere coupled to few-layer TMDs (thicker than 7 layers). Since the excitonic dipoles of WS_2 monolayers only are confined in-plane, while the local-field of NPoM with nanospheres have little components in E_x or E_y. Thus, excitonic dipoles cannot be coupled to the plasmons and strong coupling for WS_2 monolayers is not realized. Instead of nanospheres, nanocubes present a plane facet, which results in a nonnegligible local-field component besides E_z. Therefore, excitonic dipole of WS_2 monolayers can be coupled to the cavity well, resulting in the strong coupling.

In conclusion, we have successfully demonstrated a large Rabi splitting (∼145 meV) in a NPoM nanocavity coupled to the WS_2 monolayer. Monodispersed silver nanocubes and silver film constitute the plasmonic nanocavity. In the nanogap, an Al_2O_3 spacer film and a WS_2 monolayer are embedded. By adjusting the thickness of the nanogap and the size of the silver nanocubes, the plasmon resonance of the nanocavity can be easily tuned to precisely match the exciton energy of the WS_2 monolayer. A large splitting is observed from dark-field scattering spectra, which indicates a strong plasmon−exciton coupling at room temperature. The anticrossing curve is also achieved by varying the spectra overlap between SPR and exciton resonance, which further confirms the strong coupling mechanism. It presents a strong coupling platform between NPoM nanocavity and a WS_2 monolayer, which is an ideally platform to study plasmon−exciton coupling based on 2D materials and to fabricate complex structures for optical applications.

METHODS

Sample Preparation. The plasmonic nanocavity was fabricated using a bottom-up nanoassembly. First, a Ti/Silver thin film on silicon wafers are coated using election beam evaporation of a ∼10/80 nm thick. Then, Al_2O_3 spacer film was deposited on the silver-coated substrate by atomic layer deposition (ALD) at the temperature of 100 °C. WS_2 flakes were grown on sapphire substrates by CVD. Avoiding introducing dusts, we transferred WS_2 flakes from the sapphire to the Al_2O_3−silver film with the help of polydimethylsiloxane (PDMS).[42] Finally, the 65−95 nm silver nanocubes (nanoComposix, diluted to 0.01 mg/mL) were drop-cast onto the prepared substrate and rinsed off with deionized water after 1 min to remove excess nanocubes. The size distribution of the silver nanocube is shown in Figure S4. The sample was then blown dry using nitrogen gas. Silver nanocubes were monodispersed on the Al_2O_3−silver film uniformly. In order to avoid coupling among silver nanocubes, a proper distribution of nanocubes is necessary.

Optical Measurement. Dark-field scattering experiment is measured based on the microscopy (BX 53, Olympus) with a 100 W halogen lamp. The sample was illuminated by a dark-field objective (Olympus, 100×, NA = 0.9, MPLFL N). Scattered light was collected by the same objective and focused by a lens. The focus position is on the image plane, where plated a pinhole (100 μm) to choose individual nanoparticles. Then the scattered light through another lens was sent to a CCD (Qimaging, QICAM B series) or a spectrometer (Princeton Instruments Acton 2500i with Pixis CCD camera). PL signals of WS_2 monolayers were measured by a 40× objective (NA = 0.55), excited by a He−Cd laser. All experiments were measured at room temperature. The refractive indices of WS_2 monolayers are measured by a conventional ellipsometer (ME-L ellipsometer, Wuhan Eoptics Technology Co.).

ASSOCIATED CONTENT

Supporting Information

The Supporting Information is available free of charge on the ACS Publications website at DOI: 10.1021/acsphotonics.8b00931.

Calculated electric-field distribution of the plasmonic nanocavity; the refractive indices of WS_2 monolayer, simulated absorption spectra, the size distribution of the silver nanocubes, and details of splitting data listed in Figure 4c (PDF).

AUTHOR INFORMATION

Corresponding Authors

*E-mail: kale_wong@hust.edu.cn.

DOI: 10.1021/acsphotonics.8b00931
ACS Photonics 2018, 5, 3970−3976

*E-mail: lupeixiang@hust.edu.cn.

ORCID

Kai Wang: 0000-0003-2122-1294

Notes

The authors declare no competing financial interest.

■ ACKNOWLEDGMENTS

This work was supported by the 973 Programs under Grant 2014CB921301, National Natural Science Foundation of China (Nos. 11774115, 11204097, and 11674117), the Doctoral fund of Ministry of Education of China under Grant No. 20130142110078, and the Campus Science Foundation Research Project of Wuhan Institute of Technology (No. K201822). We thank Prof. Jun Zhou and Dr. Xiang Gao for assisting in preparing Al_2O_3 film. We thank Prof. Shiyuan Liu and Dr. Baokun Song for measuring the refractive indices of WS_2 monolayers. Special thanks to the Analytical and Testing Center of HUST and the Center of Micro-Fabrication and Characterization (CMFC) of WNLO for using their facilities.

■ REFERENCES

(1) Vasa, P.; Lienau, C. Strong light−matter interaction in quantum emitter/metal hybrid nanostructures. *ACS Photonics* **2018**, *5*, 2−23.

(2) Torma, P.; Barnes, W. L. Strong coupling between surface plasmon polaritons and emitters: A review. *Rep. Prog. Phys.* **2015**, *78*, 013901.

(3) Khitrova, G.; Gibbs, H. M.; Kira, M.; Koch, S. W.; Scherer, A. Vacuum Rabi splitting in semiconductors. *Nat. Phys.* **2006**, *2*, 81.

(4) Reithmaier, J. P.; Sek, G.; Loffler, A.; Hofmann, C.; Kuhn, S.; Reitzenstein, S.; Keldysh, L. V.; Kulakovskii, V. D.; Reinecke, T. L.; Forchel, A. Strong coupling in a single quantum dot-semiconductor microcavity system. *Nature* **2004**, *432*, 197−200.

(5) Smolka, S.; Wuester, W.; Haupt, F.; Faelt, S.; Wegscheider, W.; Imamoglu, A. Cavity quantum electrodynamics with many-body states of a two-dimensional electron gas. *Science* **2014**, *346*, 332−5.

(6) Piccione, B.; Aspetti, C. O.; Cho, C.-H.; Agarwal, R. Tailoring light−matter coupling in semiconductor and hybrid-plasmonic nanowires. *Rep. Prog. Phys.* **2014**, *77*, 086401.

(7) Patel, S. K.; Argyropoulos, C. Plasmonic nanoantennas: Enhancing light-matter interactions at the nanoscale. *Epj Applied Metamaterials* **2015**, *2*, 4.

(8) Liu, W.; Li, X.; Song, Y.; Zhang, C.; Han, X.; Long, H.; Wang, B.; Wang, K.; Lu, P. Cooperative enhancement of two-photon-absorption-induced photoluminescence from a 2D perovskite-microsphere hybrid dielectric structure. *Adv. Funct. Mater.* **2018**, *28*, 1707550.

(9) Chikkaraddy, R.; de Nijs, B.; Benz, F.; Barrow, S. J.; Scherman, O. A.; Rosta, E.; Demetriadou, A.; Fox, P.; Hess, O.; Baumberg, J. J. Single-molecule strong coupling at room temperature in plasmonic nanocavities. *Nature* **2016**, *535*, 127−30.

(10) Vasa, P.; Wang, W.; Pomraenke, R.; Lammers, M.; Maiuri, M.; Manzoni, C.; Cerullo, G.; Lienau, C. Real-time observation of ultrafast Rabi oscillations between excitons and plasmons in metal nanostructures with J-aggregates. *Nat. Photonics* **2013**, *7*, 128−132.

(11) Zengin, G.; Wersall, M.; Nilsson, S.; Antosiewicz, T. J.; Kall, M.; Shegai, T. Realizing strong light-matter interactions between single-nanoparticle plasmons and molecular excitons at ambient conditions. *Phys. Rev. Lett.* **2015**, *114*, 157401.

(12) Wang, H.; Toma, A.; Wang, H. Y.; Bozzola, A.; Miele, E.; Haddadpour, A.; Veronis, G.; De Angelis, F.; Wang, L.; Chen, Q. D.; Xu, H. L.; Sun, H. B.; Zaccaria, R. P. The role of Rabi splitting tuning in the dynamics of strongly coupled J-aggregates and surface plasmon polaritons in nanohole arrays. *Nanoscale* **2016**, *8*, 13445−53.

(13) Schlather, A. E.; Large, N.; Urban, A. S.; Nordlander, P.; Halas, N. J. Near-field mediated plexcitonic coupling and giant Rabi splitting in individual metallic dimers. *Nano Lett.* **2013**, *13*, 3281−6.

(14) Liu, R.; Zhou, Z. K.; Yu, Y. C.; Zhang, T.; Wang, H.; Liu, G.; Wei, Y.; Chen, H.; Wang, X. H. Strong light-matter interactions in single open plasmonic nanocavities at the quantum optics limit. *Phys. Rev. Lett.* **2017**, *118*, 237401.

(15) Wang, H.; Wang, H. Y.; Toma, A.; Yano, T. A.; Chen, Q. D.; Xu, H. L.; Sun, H. B.; Proietti Zaccaria, R. Dynamics of strong coupling between CdSe quantum dots and surface plasmon polaritons in subwavelength hole array. *J. Phys. Chem. Lett.* **2016**, *7*, 4648−4654.

(16) Santhosh, K.; Bitton, O.; Chuntonov, L.; Haran, G. Vacuum Rabi splitting in a plasmonic cavity at the single quantum emitter limit. *Nat. Commun.* **2016**, *7*, ncomms11823.

(17) Bhimanapati, G. R.; Lin, Z.; Meunier, V.; Jung, Y.; Cha, J.; Das, S.; Xiao, D.; Son, Y.; Strano, M. S.; Cooper, V. R.; Liang, L.; Louie, S. G.; Ringe, E.; Zhou, W.; Kim, S. S.; Naik, R. R.; Sumpter, B. G.; Terrones, H.; Xia, F.; Wang, Y.; Zhu, J.; Akinwande, D.; Alem, N.; Schuller, J. A.; Schaak, R. E.; Terrones, M.; Robinson, J. A. Recent advances in two-dimensional materials beyond graphene. *ACS Nano* **2015**, *9*, 11509−11539.

(18) Cong, C.; Shang, J.; Wang, Y.; Yu, T. Optical properties of 2D semiconductor WS_2. *Adv. Opt. Mater.* **2018**, *6*, 1700767.

(19) Xiao, J.; Zhao, M.; Wang, Y.; Zhang, X. Excitons in atomically thin 2D semiconductors and their applications. *Nanophotonics* **2017**, *6*, 1309−1328.

(20) Wang, S.; Li, S.; Chervy, T.; Shalabney, A.; Azzini, S.; Orgiu, E.; Hutchison, J. A.; Genet, C.; Samori, P.; Ebbesen, T. W. Coherent coupling of WS_2 monolayers with metallic photonic nanostructures at room temperature. *Nano Lett.* **2016**, *16*, 4368−74.

(21) Li, J.; Lin, Y.; Lu, J.; Xu, C.; Wang, Y.; Shi, Z.; Dai, J. Single mode ZnO whispering-gallery submicron cavity and graphene improved lasing performance. *ACS Nano* **2015**, *9*, 6794−800.

(22) Chen, R.; Li, D.; Liu, B.; Peng, Z.; Gurzadyan, G. G.; Xiong, Q.; Sun, H. Optical and excitonic properties of crystalline ZnS nanowires: Toward efficient ultraviolet emission at room temperature. *Nano Lett.* **2010**, *10*, 4956−4961.

(23) Kleemann, M. E.; Chikkaraddy, R.; Alexeev, E. M.; Kos, D.; Carnegie, C.; Deacon, W.; de Pury, A. C.; Grosse, C.; de Nijs, B.; Mertens, J.; Tartakovskii, A. I.; Baumberg, J. J. Strong-coupling of WSe_2 in ultra-compact plasmonic nanocavities at room temperature. *Nat. Commun.* **2017**, *8*, 1296.

(24) Punj, D.; Regmi, R.; Devilez, A.; Plauchu, R.; Moparthi, S. B.; Stout, B.; Bonod, N.; Rigneault, H.; Wenger, J. Self-assembled nanoparticle dimer antennas for plasmonic-enhanced single-molecule fluorescence detection at micromolar concentrations. *ACS Photonics* **2015**, *2*, 1099−1107.

(25) Long, H.; Bao, L.; Habeeb, A. A.; Lu, P. Effects of doping concentration on the surface plasmonic resonances and optical nonlinearities in AGZO nano-triangle arrays. *Opt. Quantum Electron.* **2017**, *49*, na.

(26) Zheng, D.; Zhang, S.; Deng, Q.; Kang, M.; Nordlander, P.; Xu, H. Manipulating coherent plasmon-exciton interaction in a single silver nanorod on monolayer WSe_2. *Nano Lett.* **2017**, *17*, 3809−3814.

(27) Wen, J.; Wang, H.; Wang, W.; Deng, Z.; Zhuang, C.; Zhang, Y.; Liu, F.; She, J.; Chen, J.; Chen, H.; Deng, S.; Xu, N. Room-temperature strong light-matter interaction with active control in single plasmonic nanorod coupled with two-dimensional atomic crystals. *Nano Lett.* **2017**, *17*, 4689−4697.

(28) Cuadra, J.; Baranov, D. G.; Wersall, M.; Verre, R.; Antosiewicz, T. J.; Shegai, T. Observation of tunable charged exciton polaritons in hybrid monolayer WS_2-plasmonic nanoantenna system. *Nano Lett.* **2018**, *18*, 1777−1785.

(29) Wang, M.; Krasnok, A.; Zhang, T.; Scarabelli, L.; Liu, H.; Wu, Z.; Liz-Marzan, L. M.; Terrones, M.; Alu, A.; Zheng, Y. Tunable Fano resonance and plasmon-exciton coupling in single Au nanotriangles on monolayer WS_2 at room temperature. *Adv. Mater.* **2018**, *30*, 1705779.

(30) Liu, W.; Lee, B.; Naylor, C. H.; Ee, H. S.; Park, J.; Johnson, A. T.; Agarwal, R. Strong exciton-plasmon coupling in MoS_2 coupled with plasmonic lattice. *Nano Lett.* **2016**, *16*, 1262−9.

(31) Akselrod, G. M.; Ming, T.; Argyropoulos, C.; Hoang, T. B.; Lin, Y.; Ling, X.; Smith, D. R.; Kong, J.; Mikkelsen, M. H. Leveraging

DOI: 10.1021/acsphotonics.8b00931
ACS Photonics 2018, 5, 3970−3976

nanocavity harmonics for control of optical processes in 2D semiconductors. *Nano Lett.* **2015**, *15*, 3578−84.
(32) Tan, H.; Fan, Y.; Zhou, Y.; Chen, Q.; Xu, W.; Warner, J. H. Ultrathin 2D photodetectors utilizing chemical vapor deposition grown WS2 with graphene electrodes. *ACS Nano* **2016**, *10*, 7866−73.
(33) Li, Y.; Chernikov, A.; Zhang, X.; Rigosi, A.; Hill, H. M.; van der Zande, A. M.; Chenet, D. A.; Shih, E.-M.; Hone, J.; Heinz, T. F. Measurement of the optical dielectric function of monolayer transition-metal dichalcogenides: MoS_2, $MoSe_2$, WS_2, and WSe_2. *Phys. Rev. B* **2014**, *90*, na.
(34) Liu, X.; Galfsky, T.; Sun, Z.; Xia, F.; Lin, E.-c.; Lee, Y.-H.; Kéna-Cohen, S.; Menon, V. M. Strong light−matter coupling in two-dimensional atomic crystals. *Nat. Photonics* **2015**, *9*, 30−34.
(35) Eizner, E.; Avayu, O.; Ditcovski, R.; Ellenbogen, T. Aluminum nanoantenna complexes for strong coupling between excitons and localized surface plasmons. *Nano Lett.* **2015**, *15*, 6215−21.
(36) Zhang, L.; Gogna, R.; Burg, W.; Tutuc, E.; Deng, H. Photonic-crystal exciton-polaritons in monolayer semiconductors. *Nat. Commun.* **2018**, *9*, 713.
(37) Miroshnichenko, A. E.; Flach, S.; Kivshar, Y. S. Fano resonances in nanoscale structures. *Rev. Mod. Phys.* **2010**, *82*, 2257−2298.
(38) Antosiewicz, T. J.; Apell, S. P.; Shegai, T. Plasmon−exciton interactions in a core−shell geometry: From enhanced absorption to strong coupling. *ACS Photonics* **2014**, *1*, 454−463.
(39) Lundt, N.; Klembt, S.; Cherotchenko, E.; Betzold, S.; Iff, O.; Nalitov, A. V.; Klaas, M.; Dietrich, C. P.; Kavokin, A. V.; Hofling, S.; Schneider, C. Room-temperature tamm-plasmon exciton-polaritons with a WSe_2 monolayer. *Nat. Commun.* **2016**, *7*, 13328.
(40) Lee, B.; Liu, W.; Naylor, C. H.; Park, J.; Malek, S. C.; Berger, J. S.; Johnson, A. T. C.; Agarwal, R. Electrical tuning of exciton-plasmon polariton coupling in monolayer MoS_2 integrated with plasmonic nanoantenna lattice. *Nano Lett.* **2017**, *17*, 4541−4547.
(41) Liu, X.; Bao, W.; Li, Q.; Ropp, C.; Wang, Y.; Zhang, X. Control of coherently coupled exciton polaritons in monolayer tungsten disulphide. *Phys. Rev. Lett.* **2017**, *119*, 027403.
(42) Li, B.; He, Y.; Lei, S.; Najmaei, S.; Gong, Y.; Wang, X.; Zhang, J.; Ma, L.; Yang, Y.; Hong, S.; Hao, J.; Shi, G.; George, A.; Keyshar, K.; Zhang, X.; Dong, P.; Ge, L.; Vajtai, R.; Lou, J.; Jung, Y. J.; Ajayan, P. M. Scalable transfer of suspended two-dimensional single crystals. *Nano Lett.* **2015**, *15*, 5089−97.

DOI: 10.1021/acsphotonics.8b00931
ACS Photonics 2018, 5, 3970−3976